APL/JHU CR-23

THE UNIVERSITY OF MICHIGAN
COLLEGE OF ENGINEERING
Department of Aerospace Engineering

Technical Report

AN EXPERIMENTAL AND THEORETICAL INVESTIGATION OF TWO-DIMENSIONAL JET-FLAP AERODYNAMIC INTERACTION AT SUPERSONIC SPEEDS

Norman E. Hawk and James L. Amick

ORA Project 06089

under contract with:

THE JOHNS HOPKINS UNIVERSITY
APPLIED PHYSICS LABORATORY
SILVER SPRING, MARYLAND

administered through:

OFFICE OF RESEARCH ADMINISTRATION ANN ARBOR

October 1965

Initial distribution of this report is in accordance with a list on file at the Applied Physics Laboratory, The Johns Hopkins University.

ABSTRACT

Two-dimensional jet flap aerodynamic interaction tests have been conducted in the 8 in. x 13 in. supersonic tunnel at Mach number 3.97 and Reynolds number 0.12×10^6 per inch. The test model consisted of a wedge of rectangular planform equipped with side plates and a full span jet slot. The primary data taken were jet mass flow, normal force increment due to the jet, and schlieren photographs.

The specific impulse ratios obtained varied from 3.6 at the lowest jet force parameter to 2.5 at the highest jet force parameter. (Jet force parameter is defined as the jet stagnation pressure times jet slot width, divided by free-stream pressure times body length.) For the range of variables covered in the present experiment the jet force parameter was found to govern the flow geometry, including transition in the separated shear layer.

Data on aerodynamic interaction in the case of the approximately two-dimensional, sonic jet flap have been collected from four sources. The available data for specific impulse ratio were correlated, mostly within ± 10%, over a hundredfold range of a dimensionless parameter consisting of the jet force parameter multiplied by a free stream Mach number function. An inviscid theory was developed to provide an analytical justification for the dependence on the parameter.

TABLE OF CONTENTS

	Page
LIST OF ILLUSTRATIONS	vii
LIST OF SYMBOLS	ix
INTRODUCTION	1
APPARATUS	3
EXPERIMENTAL RESULTS AND COMPARISONS WITH THEORY	6
EMPIRICAL CORRELATIONS AND PREDICTIONS OF MACH NUMBER EFFECT	13
CONCLUSIONS	20
REFERENCES	21
APPENDIX. STRONG JET THEORY	22

LIST OF ILLUSTRATIONS

Table — Page

I. Data Summary — 14

Figure

1. Model and sting assembly. — 28

2. Model and sting, interior details. — 29

3. Flow nomenclature. — 30

4. Typical schlieren pictures. — 31

5. Transition length vs. jet force parameter. — 33

6. Separation length vs. jet force parameter. — 34

7. Separation and wave angles vs. jet force parameter. — 35

8. Specific impulse ratio vs. jet force parameter, laminar separation. — 36

9. Specific impulse ratio vs. jet force parameter, turbulent separation. — 37

10. Specific impulse ratio vs. ϕ . — 38

11. Mach number predictions. — 39

12. Flow model. — 40

13. Base pressure parameter vs. Mach number. — 41

LIST OF SYMBOLS

A base pressure parameter $= \dfrac{p_\infty - p_b}{p_\infty} \dfrac{\sqrt{M_\infty^2 - 1}}{M_\infty^2}$.

A.R. jet slot aspect ratio.

C jet mass flow coefficient $= \dfrac{\dot{m}}{\dot{m}_t}$.

F_A aerodynamic force due to pressures upstream of jet.

F_j jet thrust.

h_e theoretical effective step height of jet (see Fig. 12).

I_s specific impulse due to the total normal force $= \dfrac{F_A + F_j}{\dot{m}}$.

$I_{s_{vac}}$ theoretical specific impulse of the jet in vacuum.

L length from leading edge to jet slot centerline.

$\dot{m}$ jet mass flow rate.

$\dot{m}_t$ ideal theoretical jet mass flow rate.

M Mach number.

p fluid pressure.

R jet radius of curvature (see Fig. 12).

Re_ℓ Reynolds number based on free stream conditions and length from leading edge to separation.

Re_L Reynolds number based on free stream conditions and length from leading edge to jet slot centerline.

s transition length (see Fig. 5).

t body thickness at base.

w^* width of jet throat. (Also jet exit width for sonic jets.)

ΔX separation length, length from separation to jet slot centerline.

α flow turning angle at separation (see Fig. 12).

β flow intersection angle between jet and separated shear layer (see Fig. 12).

γ ratio of specific heats.

ρ fluid density.

Subscripts:

b conditions in base region aft of jet (see Fig. 12).

j jet exit conditions.

oj jet stagnation conditions.

t inviscid theoretical values.

2 conditions in separated region ahead of jet (see Fig. 12).

∞ free stream conditions.

INTRODUCTION

It is well known that exhausting a jet laterally from a body in a supersonic stream can, due to the jet free-stream aerodynamic interaction, create a normal force on the body which is several times larger than the momentum force of the jet alone. The advent of very high speed flight has drawn increased interest to the jet as a control or force-generating device. Some attractive advantages of such a device are: (1) the successful use of jet attitude controls for spacecraft favors the simple expedient of using jet controls at all altitudes; and (2) in some cases ordinary control structures, such as fins, may be dispensed with where severe aerodynamic heating is a problem. Thus research is currently underway to provide needed data and theory for the design of jet control systems to be used at high speeds in the atmosphere.

The available theories dealing with jet free-stream interaction are all based on simplified models of the complex viscous, compressible flow. A number of these theories treat the two-dimensional case, which is a helpful simplification. In the present experiments a model was designed specifically to provide, as nearly as possible, a two-dimensional flow field for comparison with theory. This two-dimensional jet flap investigation consisted of normal force tests of a model equipped with side plates having supersonic edges. The side plates prevent lateral spillage of the flow around the obstruction created by the jet flap. The resulting flow field is a close

experimental approximation to the infinite-span, two-dimensional flow which is treated by the theories.

One of the major difficulties in the use of jet control systems is prediction of the aerodynamic interaction over a wide range of configurations, Reynolds numbers, Mach numbers, and jet free-stream pressure ratios. Consequently a large body of experimental data has accumulated as a result of efforts to understand the physical mechanisms of the aerodynamic interaction. The present report includes an attempt to unify the available data for the case of a two-dimensional sonic jet flap by means of a relatively simple inviscid dimensionless parameter.

APPARATUS

The experiments were performed in The University of Michigan 8- by 13-in. vacuum blowdown supersonic wind tunnel. The test Mach number was 3.97 and the Reynolds number approximately 120,000 per inch.

The model and sting assembly used in these tests are shown in Fig. 1. The purpose of the model design is to obtain, as nearly as possible, a two-dimensional flow situation when the jet emerges from the slot.

The model is made up of a 15° steel wedge with a Plexiglas structure fastened to it. The Plexiglas structure consists of two Plexiglas side plates (with plate glass "windows" mounted in them) and a 13° Plexiglas wedge which is supported between the two side plates at the top of the model. The upper surface of the steel wedge is blued in strips to prevent corrosion and provide markings for china clay observations. The jet slot extends the full width (3 in.) of the steel wedge and is located near the aft end of the wedge on the upper surface where the last blued (dark) strip ends. The upper surface of the steel wedge extends 6 in. forward of the slot leading edge and 0.15 in. aft of the slot trailing edge. The jet slot width (w^*) was set by means of stainless steel shim stock and then measured with a Unitron toolmaker's microscope.

Some of the details of the sting assembly are shown in Fig. 1. The sting is a tubular cantilever beam with four strain gage bridges mounted externally so as to measure bending moment at four locations along the sting. The strain gage bridges are located along the sting inside the "windshield" shown in Fig. 1.

Consolidated Electrodynamics strain gage amplifiers and recording oscillograph are used in conjunction with the strain gages. With this arrangement the effective normal force and its location can be found. The sting also carries the jet air and strain gage cooling fluid within its interior. In Fig. 1 the inlets, outlets, and solenoid valve are shown. The solenoid valve is placed near the model to obtain a rapid jet response when the valve is opened or closed.

Interior details of the model and sting are shown in Fig. 2, which is a section view taken in the plane of symmetry near the base of the steel wedge.

The jet air flows in from the right, passes through a filter before entering the jet plenum, and exhausts out the sonic jet slot. It was found that impurities in unfiltered jet air could rapidly clog a jet slot of 0.0005 in. width. With filtered jet air the slot remains immaculate (as checked by microscope) after considerable jet running time. The jet stagnation pressure is sensed downstream of the filter at the "total head port," carried aft by means of a 0.040 in. O.D. tube, and out of the sting assembly near the solenoid valve to an Ashcroft pressure gage. It was found that the jet stagnation temperature could be measured well upstream, outside the tunnel, with an error of less than 1°F.

The cooling fluid travels through annular passages, coming in from the right in Fig. 2 in the outer annulus, and returning in the inner annulus. In the present experiments, shop compressed air was used as a cooling fluid.

Additional data obtained during the tests consisted of tunnel stagnation pressure and temperature, jet mass flow rate, and schlieren pictures. Tunnel stagnation pressure was obtained using a mercury manometer connected to the

settling chamber. Jet mass flow was measured with a standard ASME sharp-edged orifice meter.

EXPERIMENTAL RESULTS AND COMPARISONS WITH THEORY

Three nominal slot widths were used in the tests. They were $w^* = 0.0005$ in., $w^* = 0.0015$ in. and $w^* = 0.0030$ in. The slots were all sonic with smooth rounded entrances from the jet plenum chamber. The range in p_{oj}/p_∞ was 45 to 1400, so that jet stagnation pressure was always much larger than tunnel free-stream pressure.

Figure 3 is a typical schlieren picture,* with some of the more important features labeled. It is well known that the effects of the jet exhausting from the slot are, in many ways, similar to the effects of a vertical step above the surface of the plate. The laminar boundary layer along the plate separates ahead of the jet to produce a separated laminar shear layer and, at the same time, a separation shock due to turning of the outer flow along with the deflected boundary layer. Beneath the shear layer is a region believed to be composed of one or more cells of circulating flow. If the jet disturbance is large, as in Fig. 3, the shear layer may undergo transition to turbulence. A case such as Fig. 3 is called "transitional," since the shear layer appears to have both laminar and turbulent regions. When p_{oj}/p_∞ is large ($p_{oj}/p_\infty = 684$ in Fig. 3) a system of jet shocks is always present. Finally, further turning of the outer flow occurs when the shear layer approaches the jet, giving rise to a jet free-stream interaction shock.

*The V-shaped pair of lines running almost vertically near the left side of the window are cracks in the 1/8 in. plate glass window. They were adequately repaired with Eastman 910 cement, and it is not believed they had any serious effect on the experimental results.

The schlieren photographs of Fig. 4 depict approximately the range of flow conditions covered in the present experiments. It should be noted that two types of schlieren pictures were taken. In one case the mercury vapor lamp was flashed, giving an exposure time of about 3 microseconds. In the other case the lamp was run continuously and the camera shutter was set at about 1/30 sec. The "slow" type of picture is characterized by smoother, more diffuse flow features and by illumination on the model. The "fast" pictures show sharper flow details and no model illumination.

The features in schlieren pictures such as those of Fig. 4 correlate well in terms of the dimensionless jet force parameter, $p_{0_j} w^* / p_\infty L$, which is proportional to the theoretical jet thrust divided by a representative aerodynamic force. The exact physical role of the denominator is obscure, and it may be possible that a more suitable non-dimensionalization will be found. For example, L could be replaced by some plausible length in the flow. The fact remains, however, that the jet force parameter has been used successfully by Amick and Carvalho (Ref. 1) and others to correlate jet interaction data. The jet force parameter also emerges as the central variable in the laminar theory of Dershin (Ref. 2). Within the range of the present experiments, all the important phenomena are governed by the jet force parameter, as will be pointed out in the following paragraphs.

Figures 4 (a) and (b) show typical flow configurations at low and high jet force parameters, respectively. The former case appears to have a laminar shear layer, whereas in the latter case transition is believed to have occurred in the shear layer at a point about two-thirds of the distance from the separation

point to the jet slot. (See Fig. 3 for greater detail.) The selection of this point as the transition point is based on the following observations: (1) near this point the shear layer turns slightly outward, indicating an increased pressure in the separated flow region; and (2) downstream of this point the shear layer appears to grow, its edges become diffuse and wavy, and a granular type of structure may be seen within the layer. Estimates of the transition distance based on similar interpretation of other schlieren pictures are plotted in Fig. 5 as a function of the jet force parameter, for three jet slot widths. Although there is a large amount of scatter in the data, the transition distance appears to correlate with the jet force parameter. Note that it was not possible to obtain data over the whole range of jet force parameter in the case of the narrowest slot. This was due to pressure limitations of the equipment. Transition is first noticed at a jet force parameter of approximately 0.10, and the length of turbulent shear layer increases as jet force parameter increases.

Returning to Figs.4 (c) and (d), we see an interesting similarity in flow geometry. The slot in Fig. 4(d) is about six times wider, the stagnation pressure is over four times smaller, and p_∞ has been increased about 17%. However, the two cases have nearly the same jet force parameter and a close resemblance to one another in flow geometry. The relationship between jet force parameter and flow geometry will later be examined in more detail.

From Figs.4(e) and (f), flow configurations at low and high jet force parameters may be compared in the case when the boundary layer is turbulent before it separates. Boundary layer turbulence was artificially induced by

fastening a 3 in. square piece of sandpaper to the upper surface of the steel wedge, just behind the leading edge. Grain size was about 0.05 in. In Figs. 4(g) and (h) the Plexiglas structure has been removed, leaving the steel wedge. Here the schlieren pictures are of higher quality due to the absence of the plate glass windows. The jet force parameter is about the same in both cases. In the second case artificial turbulence has been induced and separation delayed. (The damping strut which extends below the steel wedge is visible in Figs. 4 (g) and (h). The strut is connected to a circular plate immersed in glycerin outside the test section. The purpose of this dashpot mechanism is to damp the heavy vibrations of the model which occur with starting and stopping of the tunnel.)

Further evidence of the controlling influence of jet force parameter on the flow geometry is given in Fig. 6, where the distance from the jet forward to the separation point is plotted in dimensionless form, as a function of the jet force parameter. Like the transition data, these data were obtained by simple measurements from schlieren pictures and they show some random scatter. Since the separation "point" is not visible through the windows, its location was deduced by extending the separation shock until it intersected the upper surface of the steel wedge. The data show that the extent of the separation region increases as the jet becomes stronger, and at the highest values of jet force parameter, separation is near the leading edge. A calculation from Dershin's theory (Ref. 2) shows good agreement with the data.

Further data on flow geometry are shown in Fig. 7, where shock wave angles and separation angles are shown as a function of jet force parameter.

Again the data are rough measurements taken entirely from schlieren pictures. Since the separation angle, α, and the corresponding shock angle, θ, do not show much variation, it is difficult to draw any conclusions about their dependence on jet force parameter. However, the wave angle of the jet free-stream interaction shock, θ_j, does increase considerably as jet force parameter increases. We note in passing that θ_j was measured from a long straight segment of the shock wave, and is not representative of the initial portion of the shock near the jet. The data on angles, like the data on transition and separation lengths, do not show any consistent effect of slot width for the conditions of the present tests.

We now leave consideration of flow geometry and turn to measurements of specific impulse ratio. Figures 8 and 9 give the central results of the present tests. Here the specific impulse ratio, $I_s/I_{s_{vac}}$, is plotted as a function of the jet force parameter for three jet slot widths and for laminar and turbulent separation of the boundary layer. I_s is the total normal force, due to jet and aerodynamic interaction, divided by the measured mass flow. $I_{s_{vac}}$ is the theoretical, ideal, vacuum specific impulse resulting from the same jet geometry with the same stagnation temperature. The fact that $I_s/I_{s_{vac}}$ is greater than unity indicates an improvement over the vacuum specific impulse which is attributable to the favorable aerodynamic interaction. That is, for a given jet mass flow, one may expect a greater total normal force than the ideal jet vacuum force.

Again the data appear to be entirely a function of the jet force parameter, (particularly in the case of laminar separation) with jet slot width

variations (in many instances up to six times) having no significant ordered effect on the specific impulse ratio. For low jet force parameters a difference exists between laminar and turbulent data, while at high jet force parameters both cases merge to the same $I_s/I_{s_{vac}} \cong 2.5$.

The flagged data in Figs. 8 and 9 were taken using stainless steel side plates which were smaller than the Plexiglas plates and had no wedge across the top of the model. These tests indicate that the results are independent of side plate configuration when plates are properly designed.

In Fig. 8 several theories are compared with the laminar experimental data. The theory of Amick and Carvalho (Ref. 1) gives specific impulse ratios which are too large. Part of the discrepancy can be explained by the fact that the upper surface extended 0.15 in. behind the jet slot. However, it is estimated this effect would reduce $I_s/I_{s_{vac}}$ by only about 10% in the extreme cases. Better qualitative and quantitative agreement is obtained with the jet-flap theory of Dershin (Ref. 2). A significant aspect of Dershin's theory is the theoretical inclusion of viscous mixing along the separated shear layer. A curve calculated from the theory of Strike, Schueler, and Deitering (Ref. 3) is also included in Fig. 8. This theory gives values of specific impulse ratio which are somewhat below the present data. (A particular value of w^*/L was selected since the theory of Ref. 3 is not based solely on jet force parameter.) Finally, the strong jet theory of the Appendix is included in Fig. 8. This theory uses a very crude mathematical model and was developed as a result of successful data correlations to be discussed later in the report.

Calculations from several theories for the case of turbulent separation are compared in Fig. 9 with data taken when turbulence was artifically induced by roughness. In general the theories show fair agreement with the data. Vinson's theory (Ref. 4) shows a high interaction at low jet force parameter, contrary to the trend of the data and the other theories. However, because of the severity of the disturbance required to induce the turbulence, the present turbulent data may not be representative of that for a naturally turbulent boundary layer.

EMPIRICAL CORRELATIONS AND PREDICTIONS OF MACH NUMBER EFFECT

The experimental data of the present report, taken at constant free stream Mach number and Reynolds number, Re_L, were found to depend on the "jet force parameter," $p_{oj}w^*/p_\infty L$. Variables dependent on the jet force parameter included not only specific impulse ratio, $I_s/I_{s_{vac}}$, but also flow geometry and transition in the separated shear layer as well. If the data at this one Mach number are well correlated by a simple dimensionless parameter, then one might naturally ask if such a result is possible in the more general case when free stream Mach number and Reynolds number are varied. In this section we shall present specific impulse ratio data from Refs. 1, 3 and 5 and from the present tests, as correlated with the following parameter:

$$\phi = \frac{p_{oj}w^*}{p_\infty L} \frac{\sqrt{M_\infty^2 - 1}}{M_\infty^2}$$

The sources of data for the correlation are listed in Table I, along with information on model and jet slot configuration.

It should be mentioned in passing that in addition to the jet flap interaction data, Ref. 3 gives information on circular nozzle jet interactions and Ref. 5 presents information on solid spoilers. These data are not included in the present summary.

The jet configurations of the experiments listed in Table I are of two general types: jet spoilers, with the jet located away from the trailing edge; and jet flaps, with the jet at or near the trailing edge, as in the present tests. Jet spoiler tests, with the jet slot near the midchord, were made by

TABLE I

DATA SUMMARY

Source	M_∞	Symbol	Reynolds No., Re_L	Method of Force Measurement	w^*/L	p_{o_j}/p_∞	Slot A.R.	Jet Nozzle	Model Planform
Present Tests	3.97	◆	$Re_L = 0.72 \times 10^6$	Strain Gage Bridges	.000083 to .000500	45-1400	∞	Rounded Entrance, Sonic Exit	Rectangular 6.15" × 3"; Slot 6" from Leading Edge
Amick & Carvalho (Ref. 1)	3.95	◆	$Re_L = 0.68 \times 10^6$	Strain Gage Bridges	.001-.003	13-360	64-191	Rounded Entrance, Sonic Exit	Delta, 5.23" Chord; 60° Sweepback
Strike, Schueler, & Deitering (Ref. 3)	2.99 3.98 5.01	△ ◇ □	Total Range given: $Re_L = 3.75 \times 10^6 - 27.0 \times 10^6$	Pressure Measurements On Model Center Line	.0037-.0175	10-1000	23-107	Sharp-edged Entrance, Sonic Exit	Rectangular 15.5" × 8.5"; Slot 7.5" from Leading Edge
Heyser & Maurer (Ref. 5)	1.57 1.83 2.21 2.80	○ △ □ ◊	Total Range given: $Re_L = 1.4 \times 10^6 - 12.0 \times 10^6$	Pressure Measurements Near Model Center Line	.0039-.0118	3-60	∞ or 48-145†	Sonic Exit	Rectangular, est. 19.9cm. × 7.0cm.*; Slot 9.0cm. from Leading Edge

* Estimated from photographs.

† Depending on the effectiveness of the small side plates.

Strike, Schueler, and Deitering (Ref. 3) and Heyser and Maurer (Ref. 5). The configuration of their models was similar to that of Fig. 1, but without transparent side plates. In some of the tests of Ref. 5, small metal side plates were used. Side plates were used in the experiments of Ref. 3, but they extended downward and were not meant to contain the jet free-stream interaction.

Amick and Carvalho (Ref. 1) conducted jet flap tests with a model which was not of rectangular planform, as in all the other cases, but was a delta planform with 60° sweepback. The jet slot in this case was tapered, with the maximum slot thickness at the model centerline.

For the purposes of the present correlation the jet spoiler results listed above will be treated as jet flap data simply by considering only the forces measured ahead of the jet. Probably the essential difference between the two types of flow is in the pressure downstream of the jet exit, and the effect it has upon jet curvature. The theory of Amick and Carvalho (Ref. 1) showed that a small change in this pressure had a small effect on the specific impulse ratio, $I_s/I_{s_{vac}}$. This seems a plausible result because the pressure just upstream of the jet is generally much larger than p_∞ and the pressure on the downstream side of the jet drops to a fraction of p_∞. (See Ref. 3, Fig. 12, for example.) Therefore, the jet curvature and the upstream flow field are not likely to be influenced greatly by the downstream model configuration.

It is interesting to note from Table I the total range of parameters for all the references combined:

$$M_\infty : 1.57 - 5.01$$

$$Re_L : 0.68 \times 10^6 - 27 \times 10^6$$

$$w^*/L \;:\; 8.3 \times 10^{-5} - 1.75 \times 10^{-2}$$

$$p_{oj}/p_\infty \;:\; 3 - 1400$$

Figure 10 gives $I_s/I_{s_{vac}}$, a variable of primary importance to the fuel economy of a jet flap, as a function of the parameter Φ defined above. Figure 10 is only for the case of "natural" boundary layers, either laminar or turbulent, on smooth model surfaces. The artificially turbulent data taken in the present report and Ref. 1 would not correlate well in Fig. 10, falling somewhat below the other data at low values of Φ.

All the data of Fig. 10 are for two-dimensional and nearly two-dimensional jet flap configurations at supersonic speeds. The data from Ref. 5 (Heyser and Maurer) were taken from their Fig. 26(b), which is for the case with side plates. The data of Ref. 3 (Strike, Schueler, and Deitering) were taken from their Fig. 32. Although side plates were not used in Ref. 3, aerodynamic force was determined from pressure measurements along the centerline where two-dimensional values are most closely approached. The Ref. 3 data in Fig. 10 is for slot A.R. = 53 or larger. Both Ref. 3 and Ref. 5 give data in terms of the force magnification F_A/F_j, where F_A is the aerodynamic force due to the pressures upstream of the jet and F_j is the jet thrust. To convert the force magnification to the specific impulse ratio we simply add one. This can be shown beginning with an approximate definition of specific impulse ratio for $p_{oj}/p_\infty \gg 1$:

$$\frac{I_s}{I_{s_{vac}}} \cong \frac{(F_A + F_j)/\dot{m}}{F_{jt}/\dot{m}_t} = \frac{F_A + F_j}{(\dot{m}/\dot{m}_t)F_{jt}} \qquad (1)$$

Now if we assume (as in Ref. 3) that

$$\frac{F_j}{F_{jt}} \simeq \frac{\dot{m}}{\dot{m}_t} = C$$

then it immediately follows

$$\frac{I_s}{I_{s_{vac}}} \simeq \frac{F_A}{F_j} + 1 \, . \tag{2}$$

C is usually near unity; however, in the present experiments, where a narrow 0.0005 in. jet slot was used, values as low as C = 0.6 were measured. In Ref. 3 the lowest measured value of C was about 0.7 for rectangular slots with sharp-edged entrances.

The empirical relation given in Fig. 10 is

$$\frac{I_s}{I_{s_{vac}}} = \log_{10}\left(\frac{13.02}{\phi 1.18}\right) \tag{3}$$

Most of the data are within ± 10% of Eq. (3). This correlation is apparently valid over a large range of Reynolds numbers. Although it was not possible to determine separation Reynolds numbers corresponding to individual points in Fig. 10, it is known that turbulent boundary layer separation occurred in some of the data of Ref. 3 and in a large portion of the data of Ref. 5.* Reference 1 had laminar separations, except in the cases (not shown) where turbulence was artificially induced.

*This was found by examining schlieren pictures and streamwise surface pressure profiles.

In addition to the correlation given in Fig. 10, Ref. 6 (Hawk and Amick) presents correlations of flow geometry as a function of Φ. The results are inconclusive because of lack of sufficient two-dimensional data at several Mach numbers.

Also shown in Fig. 10 are predictions of specific impulse ratio for $M_\infty = 2$ and $M_\infty = 5$ using the strong jet theory (Appendix). The theory does not provide close agreement with data, although it shows the correct trend and fair agreement over a hundredfold range in the parameter Φ.

An extension of Eq. (3) to higher Mach numbers is presented in Fig. 11. Considering the successful specific impulse correlation from Mach number 1.57 to 5.01 and the current interest in specific impulse ratios at higher Mach numbers, it was felt that a projection of Eq. (3) to higher Mach numbers would be worthwhile. Therefore, in Fig. 11 the specific impulse ratio is plotted from Eq. (3) as a function of M_∞ up to $M_\infty = 8$. Specific values of p_{oj}/p_∞, w^*/L, and Reynolds number were selected in order to make calculations from a number of theories.

The prediction according to the theory of Strike, Schueler, and Deitering (Ref. 3) starts below the empirical result in Fig. 11 and shows a more rapid increase in specific impulse ratio with Mach number. This theory, using empirical boundary layer separation results, predicts little difference in specific impulse ratio between laminar and turbulent separation. On the other hand, the theory of Amick and Carvalho (Ref. 1), which is also based on empirical separation laws, shows a large difference between the two cases. The turbulent theory of Ref. 1 gives fair agreement with Eq. (3), particularly

at the lower Mach numbers. The laminar separation theory of Dershin (Ref. 2), which includes the effects of mixing along the separated shear layer, gives a decrease in specific impulse ratio as M_∞ increases, contrary to the trend of Eq. (3) and the other theories. The same is true of Dershin's turbulent theory (Ref. 2). Vinson's theory (Ref. 4) shows reasonably good agreement with Eq.(3) over the entire range of Mach number. It is interesting that, although the theories show differing results for a given physical situation, most of them predict the same trend of increasing aerodynamic interaction as Mach number increases.

CONCLUSIONS

As a result of the present experimental and theoretical investigation of two-dimensional jet aerodynamic interaction, the following conclusions are made:

1. At $M_\infty = 3.97$ and $Re_L = 720{,}000$, the two-dimensional aerodynamic interaction produces a specific impulse ratio which is approximately constant at 2.5, for either laminar or turbulent separation, for jet force parameters between 0.12 and 0.40. At lower jet force parameters the specific impulse ratio increases for laminar separation, reaching 3.6 at a jet force parameter of 0.04.

2. Over the entire range of jet force parameter and slot width covered, slot width has no significant effect on the specific impulse ratio, except insofar as it enters the jet force parameter in the form $p_{oj}w^*/p_\infty L$.

3. For the range of variables covered in the present experiments (at constant Mach No. and Reynolds No.) the jet force parameter is an important quantity governing the flow geometry (including shear layer transition) and the specific impulse ratio.

4. For sonic jet flaps and spoilers, data on specific impulse ratio from four sources were found to correlate with the dimensionless parameter, Φ, to within $\pm$ 10% of an empirical rule when boundary layer transition occurred naturally on a smooth surface.

5. An inviscid, empirical theory has been developed to provide further evidence favoring the importance of Φ as a correlation parameter.

REFERENCES

1. Amick, J. L. and Carvalho, G. F., "Interaction Effects of a Jet Flap on a 60° Delta Wing at Mach Number 4, and Comparison with Two-Dimensional Theory," University of Michigan, College of Engineering, Technical Report CM-1031, February, 1963.

2. Dershin, H., "Forces Due to Gaseous Slot Jet Boundary-Layer Interaction," Journal of Spacecraft and Rockets, Vol. 2, No. 4 (July-August 1965), pp. 597-599.

3. Strike, W. T., Schueler, C. J., and Deitering, J. S., "Interactions Produced by Sonic Lateral Jets Located on Surfaces in a Supersonic Stream," AEDC-TDR-63-22, April, 1963.

4. Vinson, P. W., "Prediction of Reaction Control Effectiveness at Supersonic and Hypersonic Speeds," Martin-Orlando Report OR 6487, March 1965.

5. Heyser, A. and Maurer, F., "Experimental Investigations on Solid Spoilers and Jet Spoilers at Mach Numbers of 0.6 to 2.8," Jet Propulsion Laboatory, C.I.T., Translation No. 32, February, 1964, or Zeitschrift fur Flugwissenschaften, Vol. 10, Nos. 4, 5, 1962.

6. Hawk, N. E. and Amick, J. L., "An Empirical Correlation of Jet-Flap Aerodynamic Interaction Data at Mach Numbers 1.57 to 5.01 and Comparisons with Theory (Preliminary)," University of Michigan Wind Tunnel Memo No. 282, November, 1964.

7. Chapman, D., "An Analysis of Base Pressure at Supersonic Velocities and Comparison with Experiment," N.A.C.A. Report 1051, 1951.

8. Gadd, G. E., Holder, D. W., and Regan, J. D., "Base Pressure in Supersonic Flow," A.R.C. C.P. No. 271, 1956.

APPENDIX

STRONG JET THEORY

Because of the correlation of $I_{s/I_{svac}}$ with the dimensionless parameter ϕ over a large range of free stream Reynolds numbers, it seems plausible that a simple inviscid momentum analysis based on ϕ should give agreement with experiment.

Consider the idealized model shown in Fig. 12. The term "strong jet" is applied to this model because it is assumed that $p_{oj/p_\infty} \gg 1$ and the effective step height of the jet is so large that the separation extends to the leading edge. This simplification eliminates the variable ΔX, which is replaced here by the constant L. Figure 6 shows that in the present experiments the two-dimensional laminar separation is near the leading edge when $\frac{p_{oj} w^*}{p_\infty L} \geq 0.40$. At this point, $\phi \cong 0.1$ which is midway through the logarithmic range of ϕ for which data could be found. Note that although separation is near the leading edge, α may remain small (see Fig. 7). In the strong jet theory α is assumed to be a small angle.

From weak shock theory we have

$$\frac{p_2 - p_\infty}{p_\infty} \cong \frac{\gamma_\infty M_\infty^2 \alpha}{\sqrt{M_\infty^2 - 1}} \qquad \text{(A-1)}$$

We assume a thin jet with constant radius of curvature which is controlled by the initial transverse pressure gradient:

$$\frac{\rho_j V_j^2}{R} = \frac{p_2 - p_b}{w^*} \qquad \text{(A-2)}$$

Both (A-1) and (A-2) are based on conservation of momentum. Using (A-1), (A-2), and $\rho_j V_j^2 = \gamma_j p_j M_j^2$, one gets for the isentropic jet

$$\frac{R}{L} = \frac{\gamma_j k_1(M_j)\phi}{\gamma_\infty \alpha + A} \qquad \text{(A-3)}$$

where

$$k_1(M_j) = M_j^2 \left(1 + \frac{\gamma_j - 1}{2} M_j^2\right)^{\gamma_j/(1 - \gamma_j)}$$

and

$$A = \left(\frac{p_\infty - p_b}{p_\infty}\right) \frac{\sqrt{M_\infty^2 - 1}}{M_\infty^2}$$

Now from the geometry we have

$$R = {}^{h_e}/_{\sin \delta}$$

and if α is small,

$$\alpha \simeq {}^{h_e}/_{L} \ .$$

(A-3) becomes

$$\gamma_\infty \left(\frac{h_e}{L}\right)^2 + A \left(\frac{h_e}{L}\right) = \gamma_j k_1 \phi \sin \delta \ . \qquad \text{(A-4)}$$

Again from the geometry we have

$$\delta = {}^{\pi}/_{2} - (\alpha + \beta)$$

and taking the sine we have for small α,

$$\sin \delta \cong \cos \beta - \alpha \sin \beta \quad . \tag{A-5}$$

Substituting (A-5) into (A-4) one gets

$$\left(\frac{h_e}{L}\right)^2 + \left(\frac{\gamma_j}{\gamma_\infty} k_1 \phi \sin \beta + \frac{A}{\gamma_\infty}\right)\left(\frac{h_e}{L}\right) - \frac{\gamma_j k_1}{\gamma_\infty} \phi \cos \beta = 0$$

or

$$\left(\frac{h_e}{L}\right) = -\left(\frac{\gamma_j}{\gamma_\infty} \frac{k_1 \phi \sin \beta}{2} + \frac{A}{2\gamma_\infty}\right) + \sqrt{\left(\frac{\gamma_j}{\gamma_\infty} \frac{k_1 \phi \sin\beta}{2} + \frac{A}{2\gamma_\infty}\right)^2 + \frac{\gamma_j}{\gamma_\infty} k_1 \phi \cos \beta.} \tag{A-6}$$

Now the aerodynamic force is given by

$$F_A = (p_2 - p_\infty)L = \gamma_\infty \left(\frac{h_e}{L}\right) \frac{p_\infty M_\infty^2 L}{\sqrt{M_\infty^2 - 1}} \tag{A-7}$$

and the ideal jet force is given by,

$$F_j = k_2(M_j) p_{oj} w^* \tag{A-8}$$

where

$$k_2(M_j) = \left(\frac{2}{\gamma_j+1}\right)^{\frac{1}{2}\left(\frac{\gamma_j+1}{\gamma_j-1}\right)} \left(\frac{1+\gamma_j M_j^2}{M_j}\right) \Big/ \sqrt{1 + \frac{\gamma_j - 1}{2} M_j^2}$$

for $p_{oj}/p_\infty \gg 1$. Thus

$$\frac{F_A}{F_j} = \frac{\gamma_\infty}{k_2} \frac{1}{\phi} \left(\frac{h_e}{L}\right) \tag{A-9}$$

It is then assumed that

$$I_s/I_{s_{vac}} \simeq \frac{F_A}{F_j} + 1. \qquad (10)$$

For the sonic air jets dealt with in this report one has,

$$\gamma_j = \gamma_\infty = 1.4$$

$$k_1 = 0.528$$

$$\gamma_\infty/k_2 = 1.104.$$

Equations (A-6), (A-9), and (A-10) constitute a solution if β and A are given.

With regard to β and A, reasonable success may be obtained by assigning them appropriate constant values (see Refs. 1 and 6). However, it is felt that predictions of Mach number effect can be improved by allowing variations, particularly in the case of A. Figure 13 gives data on A from a variety of sources. The maximum possible value of A is represented by $p_b = 0$. (Chapman, Ref. 7, points out that the limit to minimum base pressure is determined by the maximum deflection angle for shock attachment at the wake neck. However, this limitation is nearly the same as $p_b = 0$ for supersonic Mach numbers.) The data shown here follow the trend of the maximum curve of A in a rough fashion. The values of A obtained behind jets (Refs. 3 and 5) are based on the minimum pressure in downstream profile. For our purposes A is taken to be:

$$A = (0.7)\ \frac{\sqrt{M_\infty^2 - 1}}{M_\infty^2} \qquad (A\text{-}11)$$

Equation (A-11) neglects the effects of body shape, Reynolds number, and jet

configuration on the effective base pressure. Nevertheless it is a better approximation than A = constant.

Proper evaluation of β, the flow intersection angle, appears to be even more difficult. Where the free stream intercepts the jet, the jet free-stream interaction shock causes a pressure discontinuity. In the present mathematical model the pressure controls jet curvature, hence the jet slope will not be abruptly changed and the free stream must initially turn through the angle β.

There is little experimental data on which to base a selection of β. Amick and Carvalho (Ref. 1) studied the supersonic data of Ref. 8 on the flow intersection angle between shear layers in the base region behind two-dimensional bodies. They found that β, as deduced from base pressure, depended on the nature of the separated shear layer. That is, for a purely laminar shear layer, $\beta = 10°$ is a representative value; for a transitional layer $\beta = 50°$, and for a fully turbulent separated shear layer $\beta = 40°$. Whether or not base pressure data and the concept of a simple flow intersection angle are applicable to the confluence of a free shear layer and an expanding jet are questions which require more study. In most of the jet flap data of current interest, the separated shear layer ahead of the jet is turbulent or transitional (see Fig. 5, for example), so constant β in the range of $40° - 50°$ has sometimes been selected (see Refs. 1 and 6). Note, however, that if the free stream turns by more than $45.6°$, a detached shock will result even when M_2 is infinite. A detached jet free-stream interaction shock will cause a pressure discontinuity along the separated shear layer which is inconsistent with the assumption of a constant pressure separated region. Therefore it is assumed

that the free stream initially turns an amount, β, which is always equal to the maximum deflection angle determined by M_2.

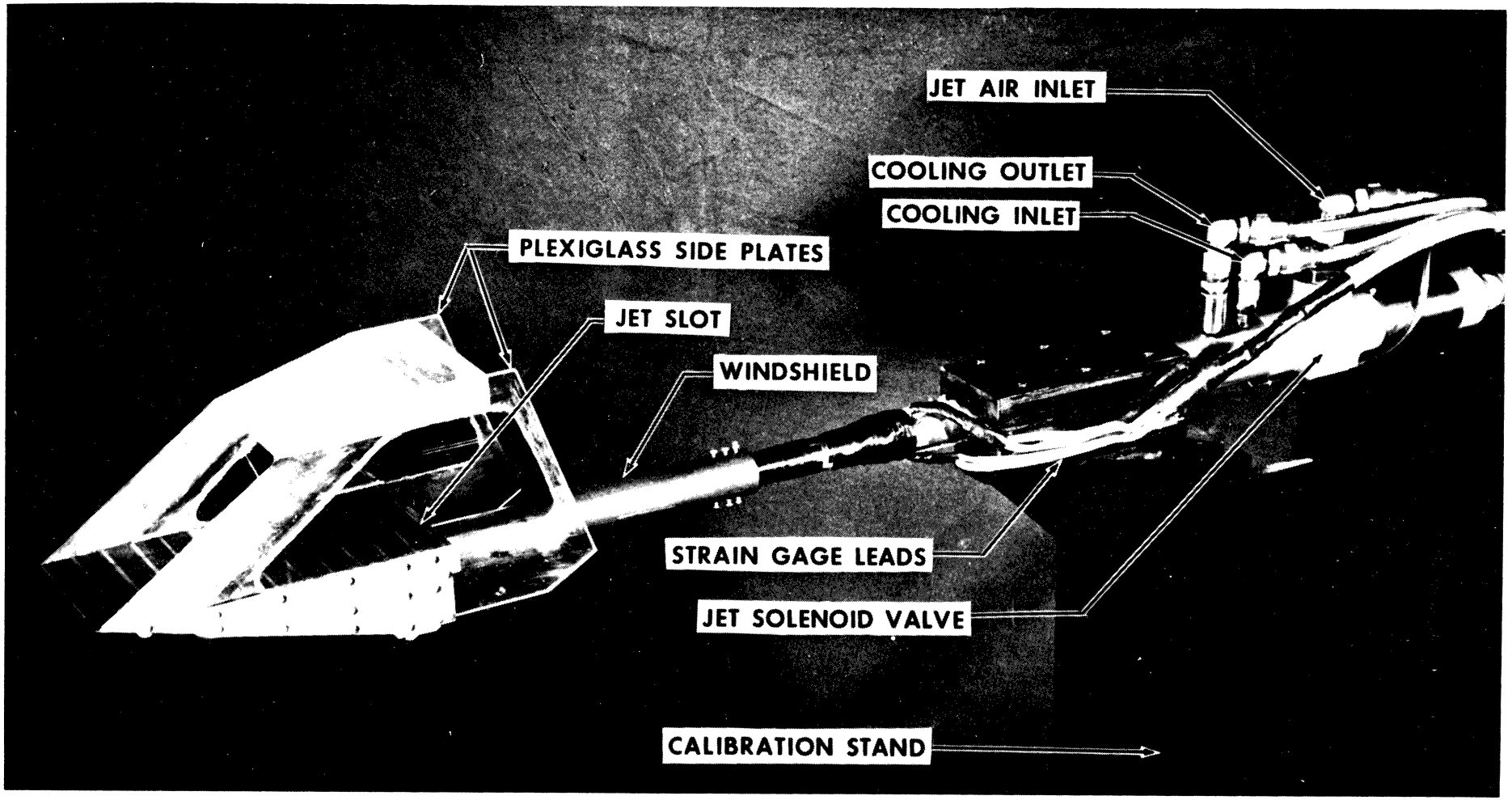

Fig. 1. Model and sting assembly.

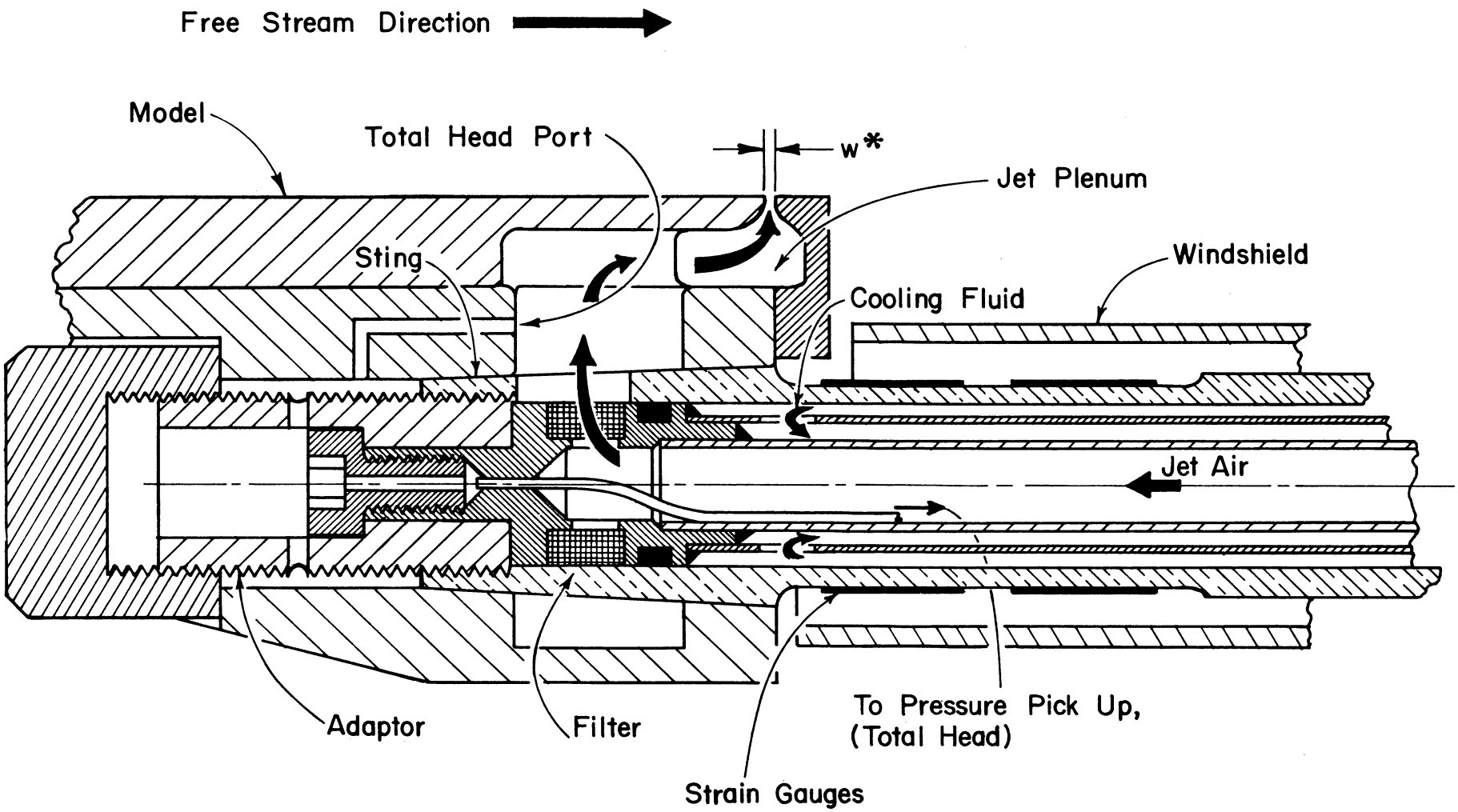

Fig. 2. Model and sting, interior details.

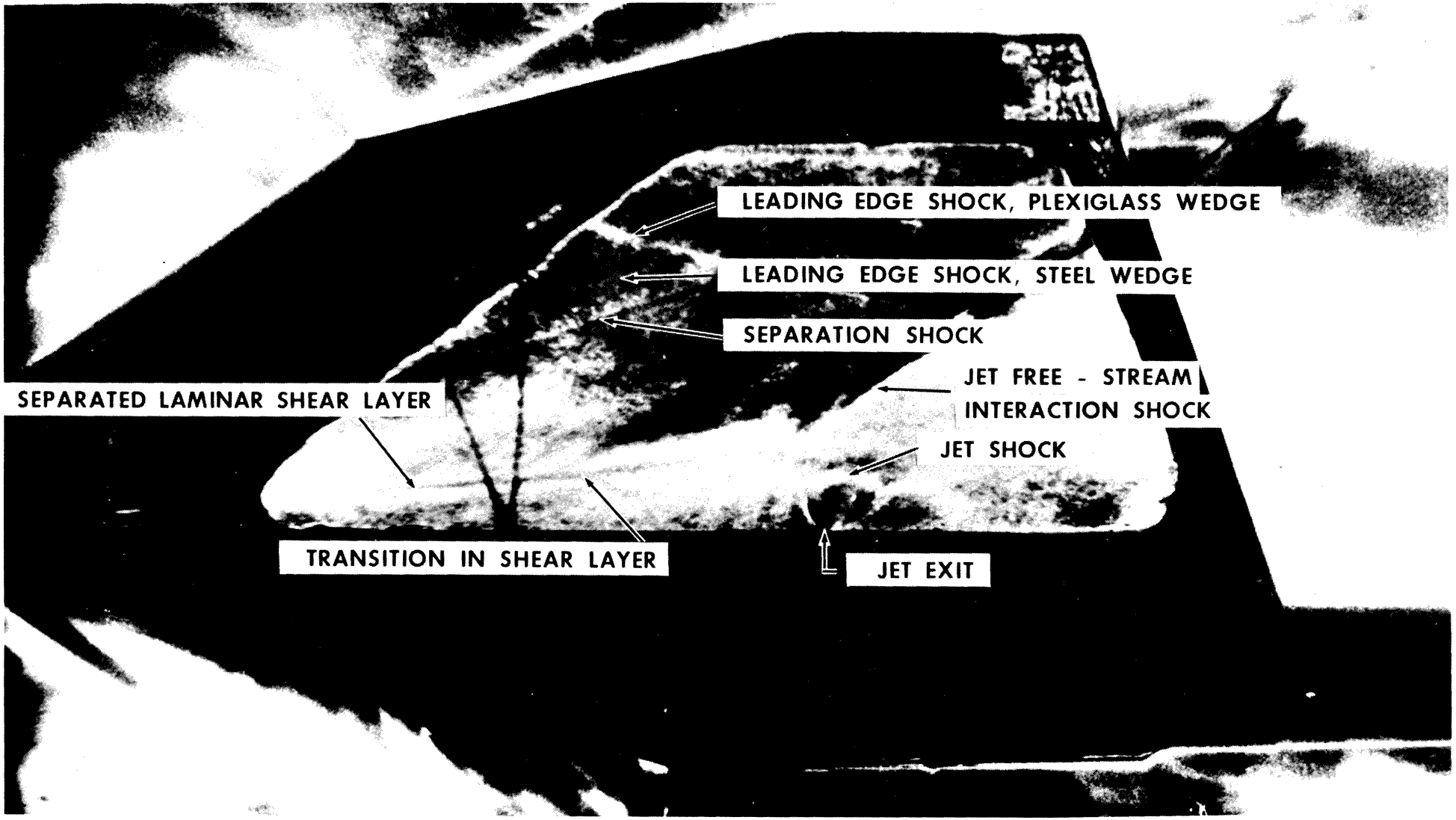

Fig. 3. Flow nomenclature.

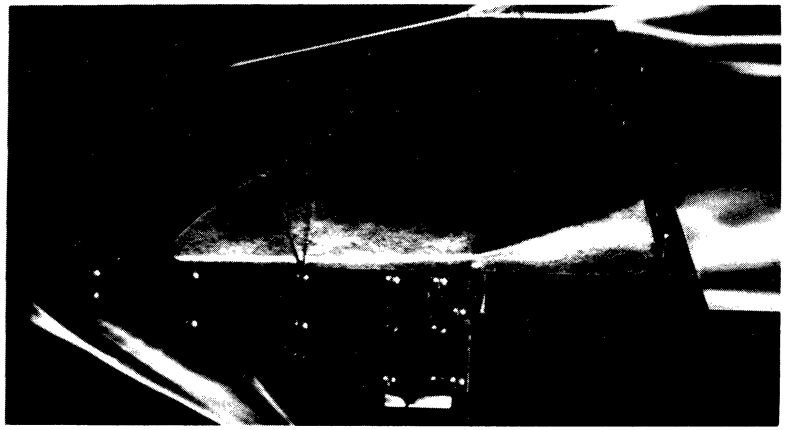

(a) $p_{0_j} = 52.6$ psia, $w^* = .0005"$, $p_{0_j} w^* / p_\infty L = .047$
Laminar separation

(b) $p_{0_j} = 63.9$ psia, $w^* = .0031"$, $p_{0_j} w^* / p_\infty L = .342$
Laminar separation

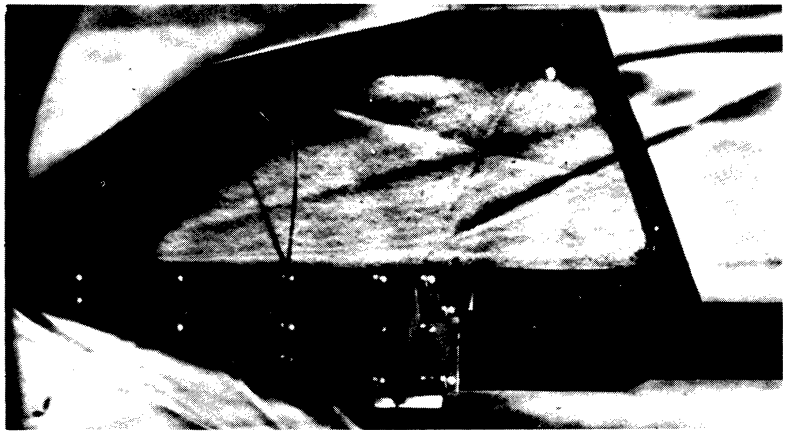

(c) $p_{0_j} = 104.5$ psia, $w^* = .0005"$, $p_{0_j} w^* / p_\infty L = .109$
Laminar separation

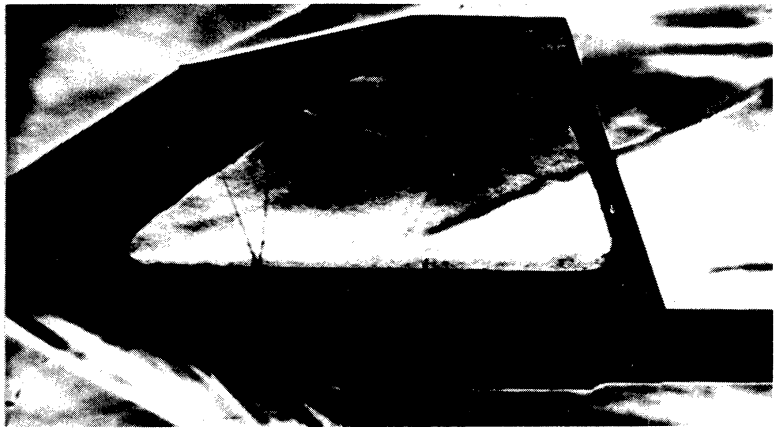

(d) $p_{0_j} = 22.9$ psia, $w^* = .0031"$, $p_{0_j} w^* / p_\infty L = .123$
Laminar separation

Fig. 4. Typical schlieren pictures.

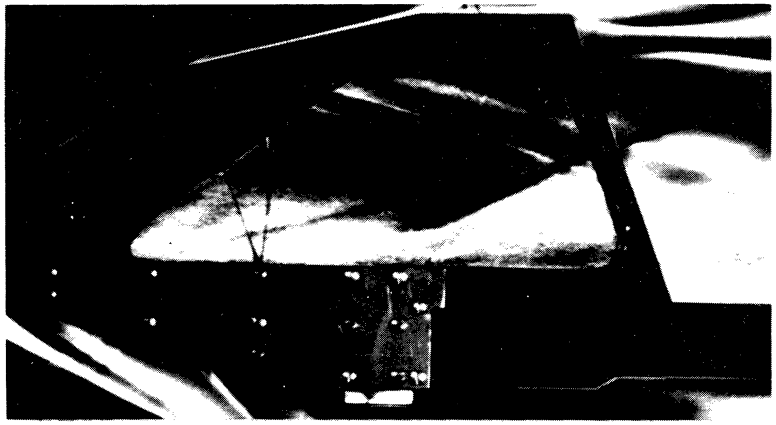

(e) p_{0_j} = 102.5 psia, w^* = .0005", $p_{0_j} w^*/p_\infty L$ = .092
Turbulent separation

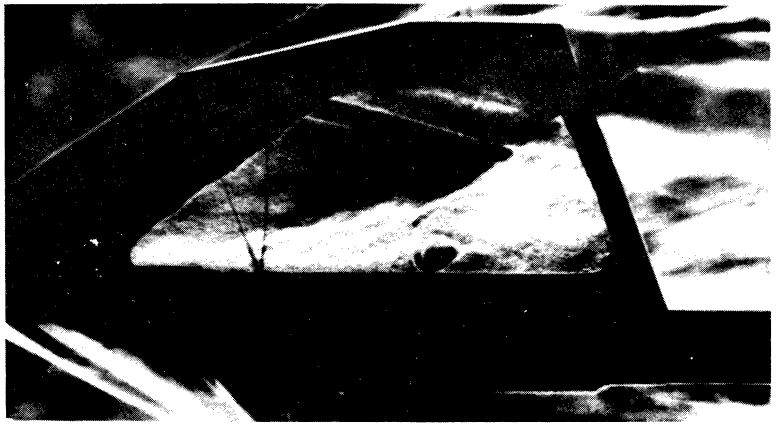

(f) p_{0_j} = 69.2 psia, w^* = .0031", $p_{0_j} w^*/p_\infty L$ = .369
Turbulent separation

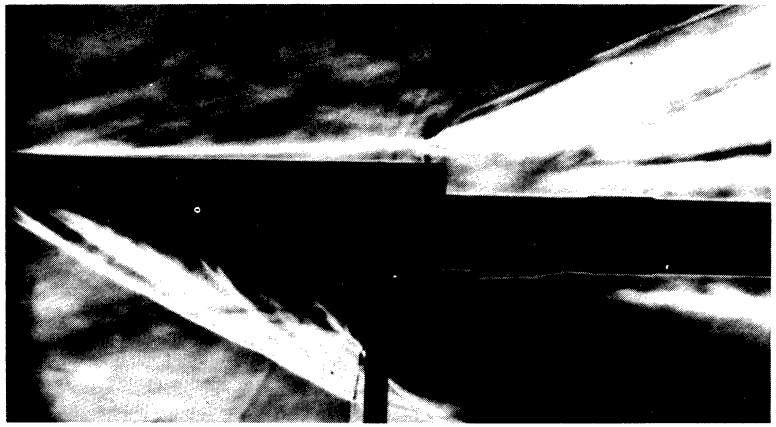

(g) p_{0_j} = 101.8 psia, w^* = .0005", $p_{0_j} w^*/p_\infty L$ = .091
Laminar separation

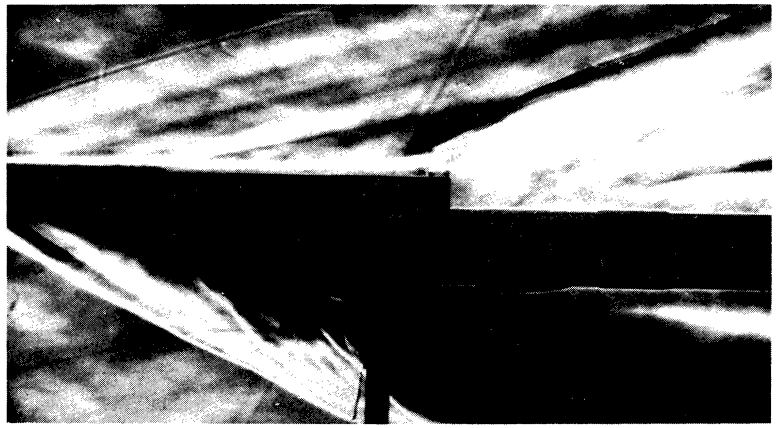

(h) p_{0_j} = 103.5 psia, w^* = .0005", $p_{0_j} w^*/p_\infty L$ = .093
Turbulent separation

Fig. 4. (Concluded).

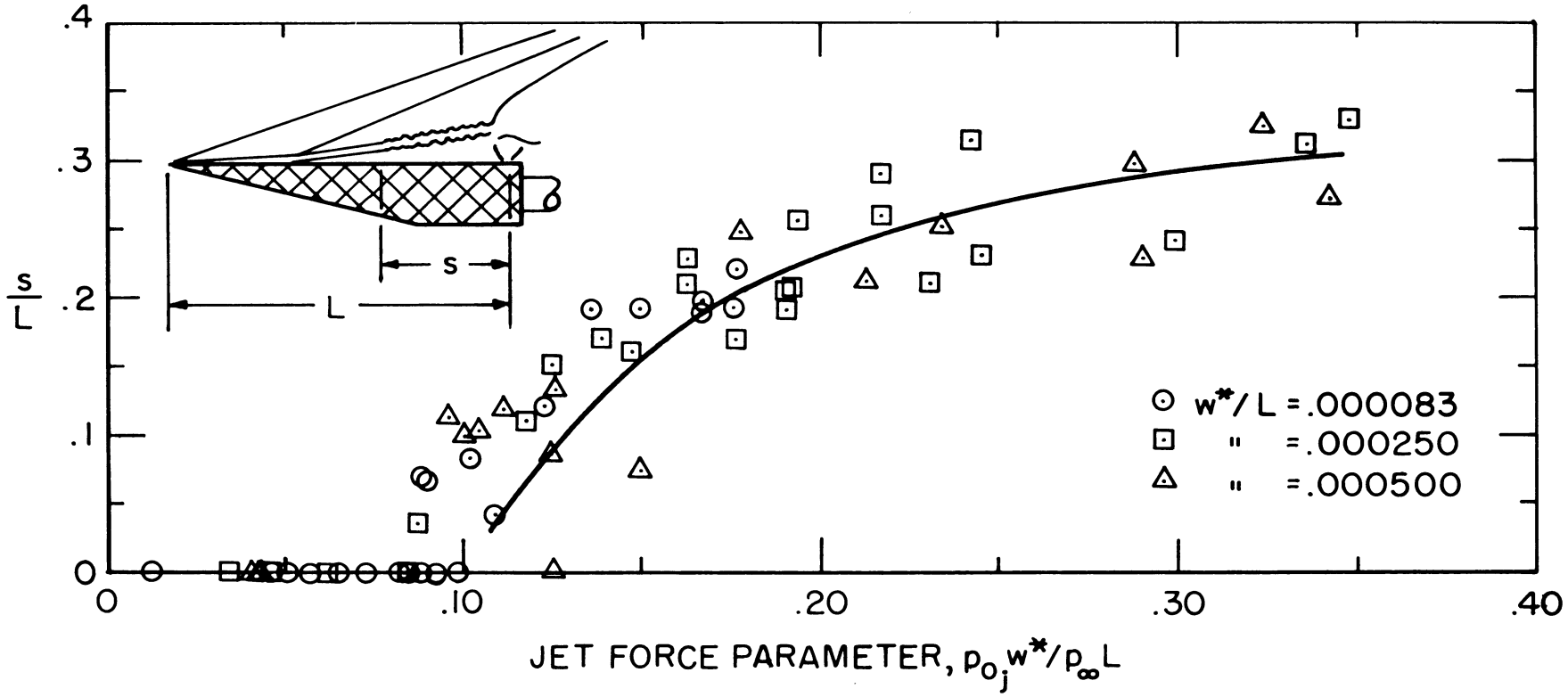

Fig. 5. Transition length vs. jet force parameter.

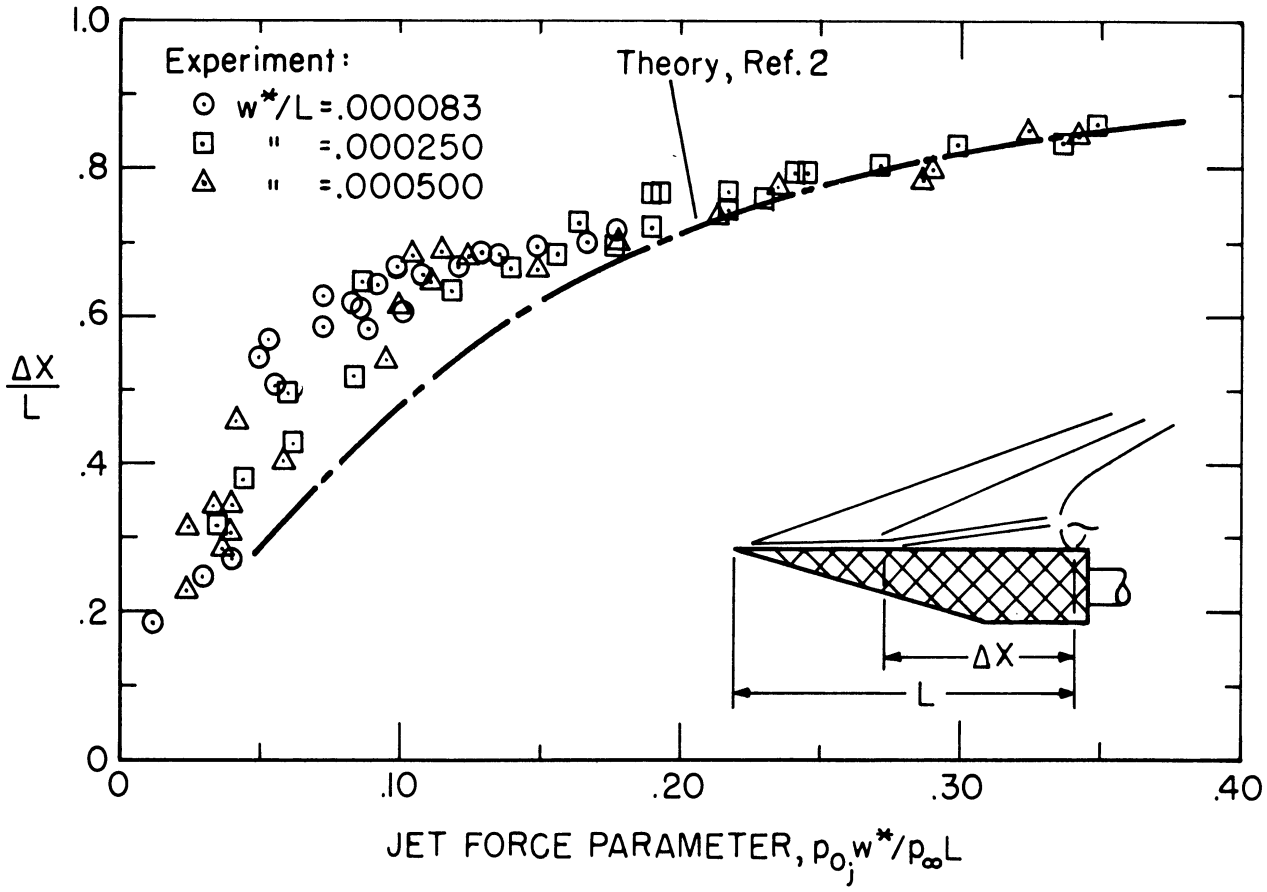

Fig. 6. Separation length vs. jet force parameter.

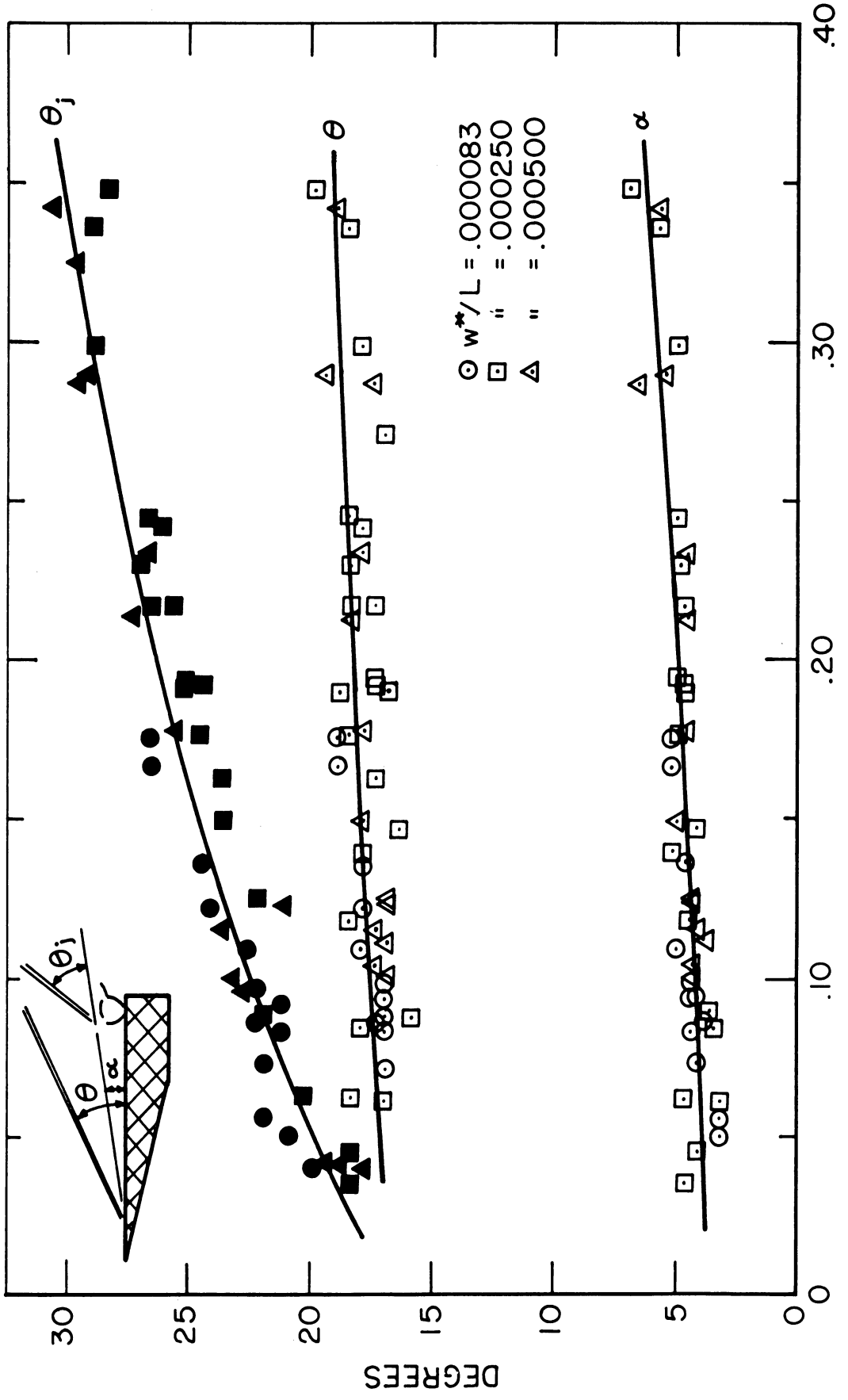

Fig. 7. Separation and wave angles vs. jet force parameter.

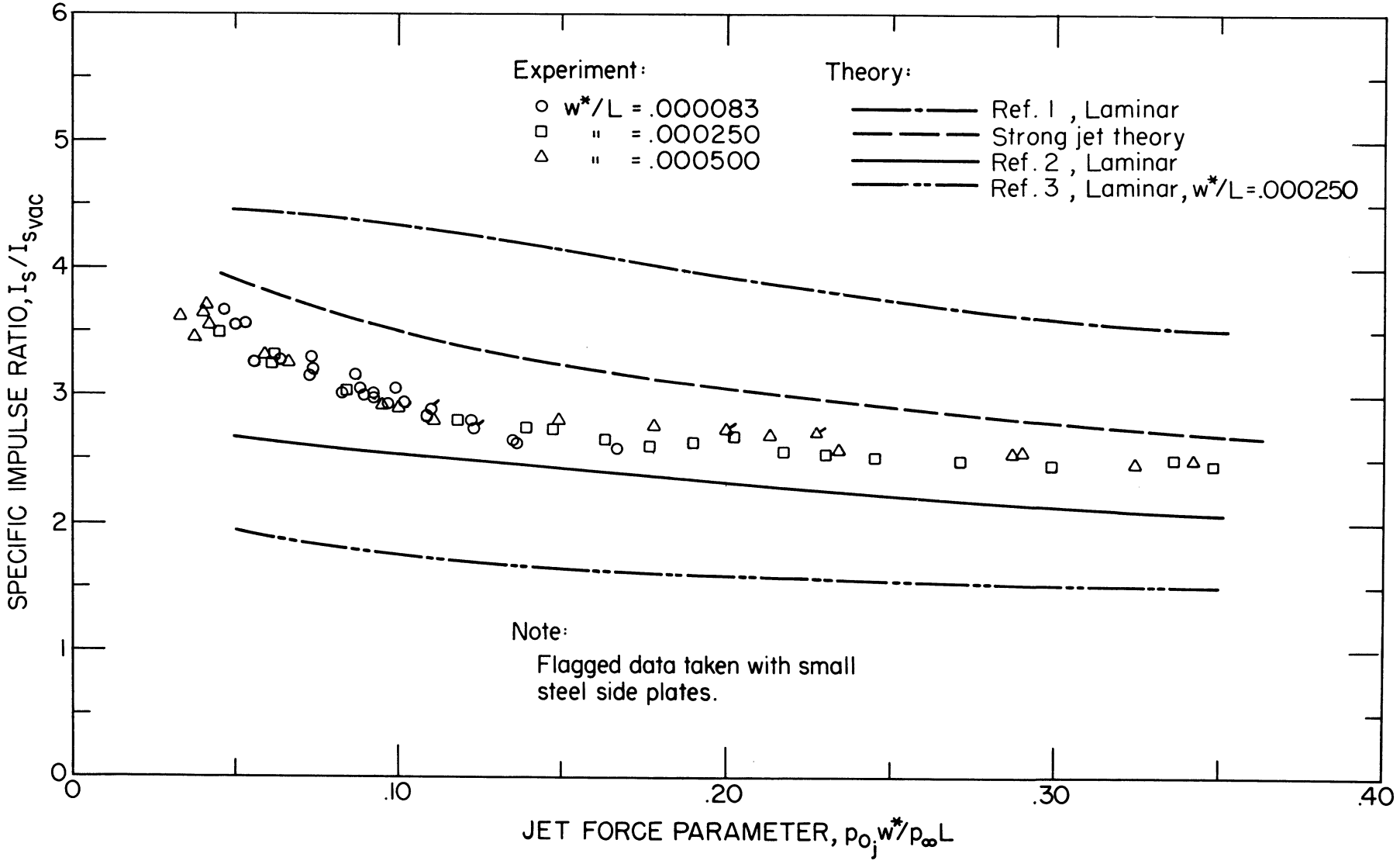

Fig. 8. Specific impulse ratio vs. jet force parameter, laminar separation.

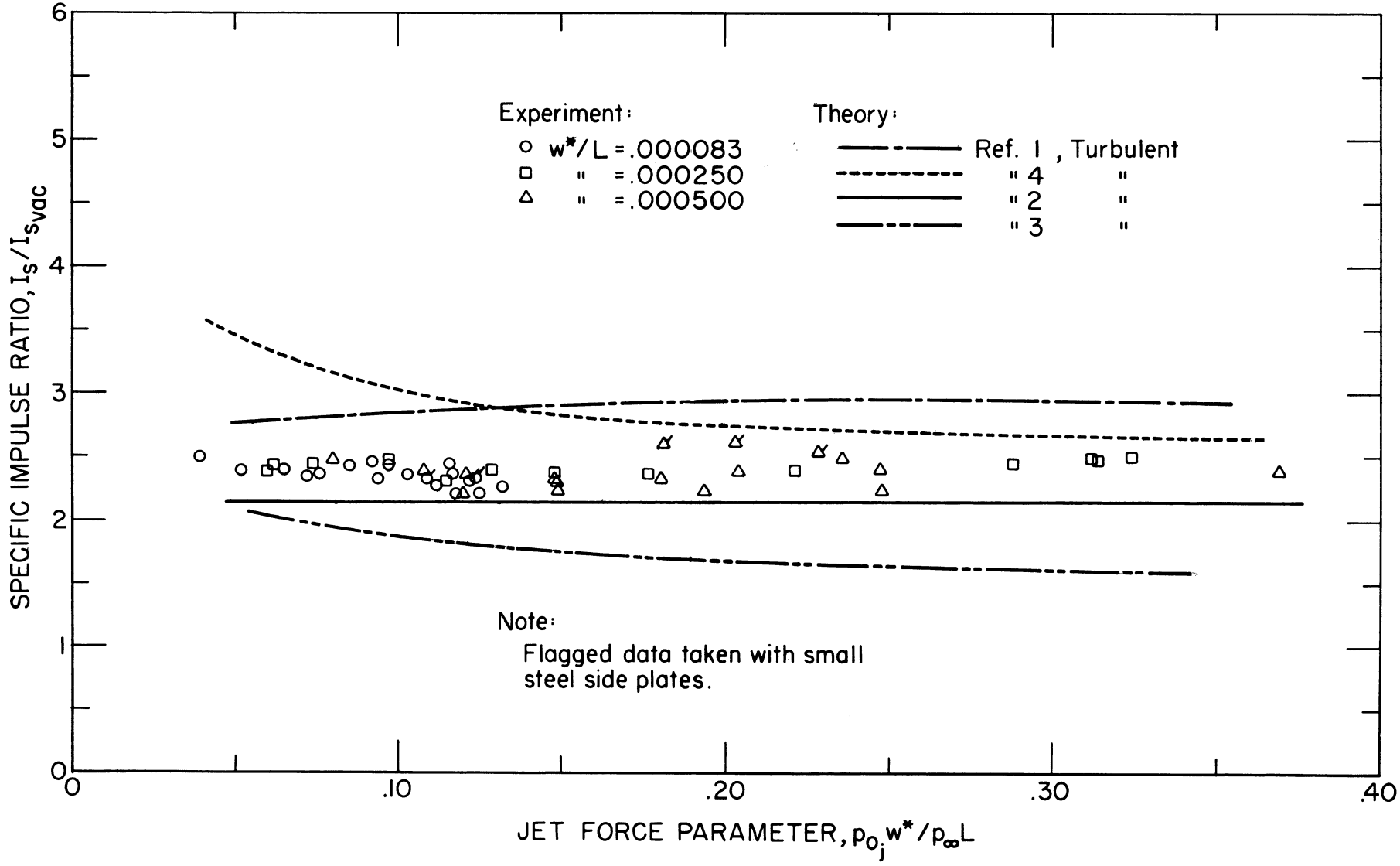

Fig. 9. Specific impulse ratio vs. jet force parameter, turbulent separation.

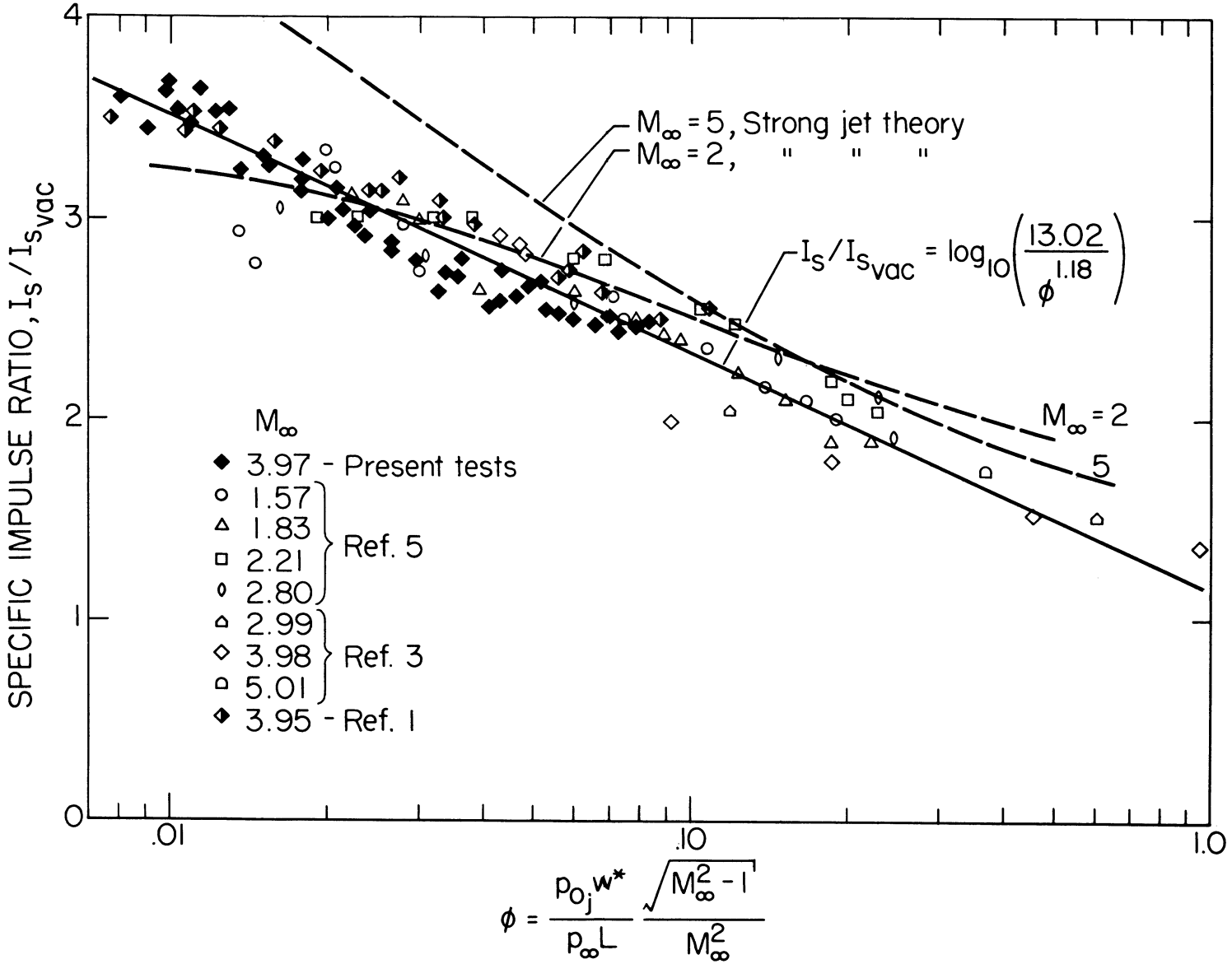

Fig. 10. Specific impulse ratio vs. ϕ.

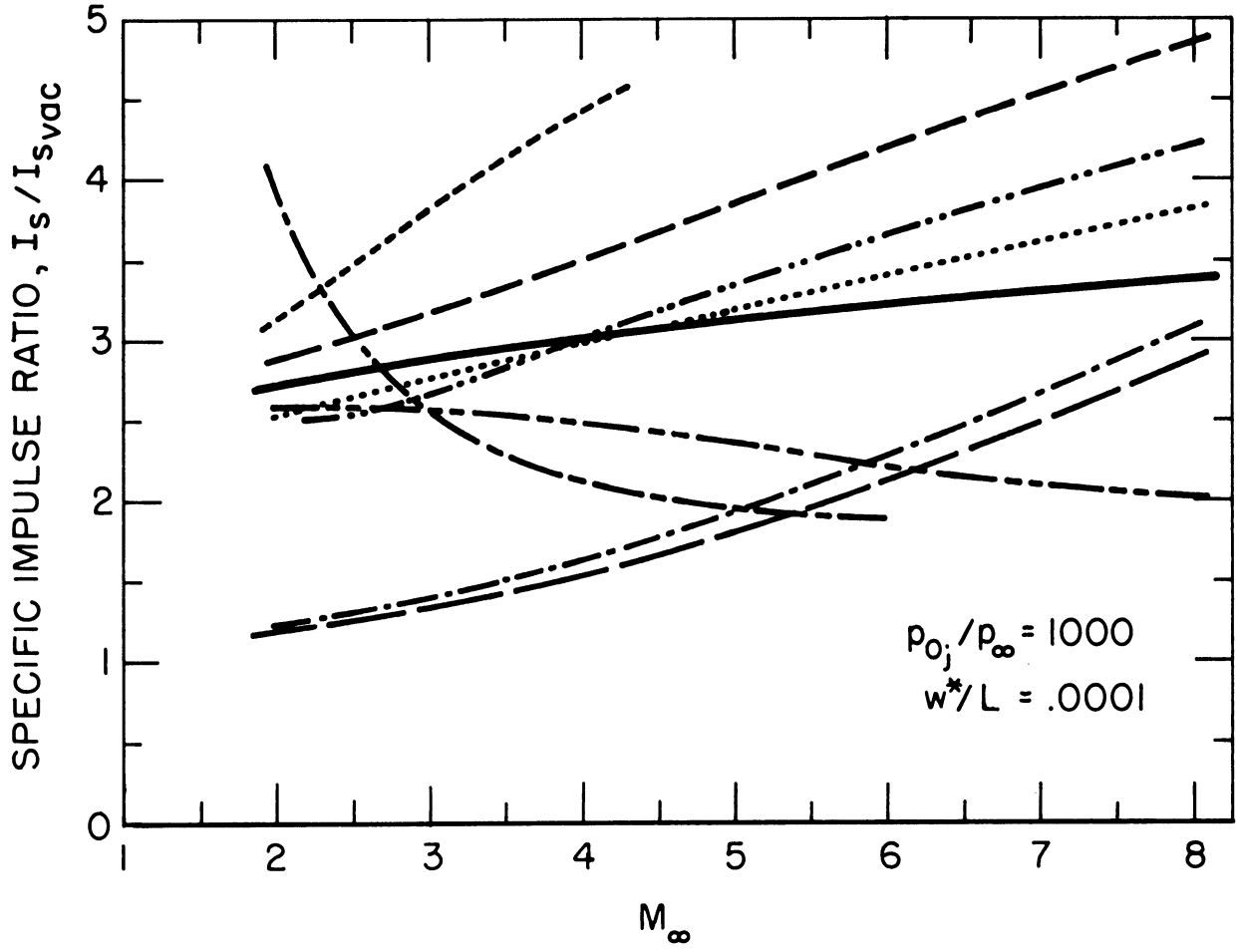

Fig. 11. Mach number predictions.

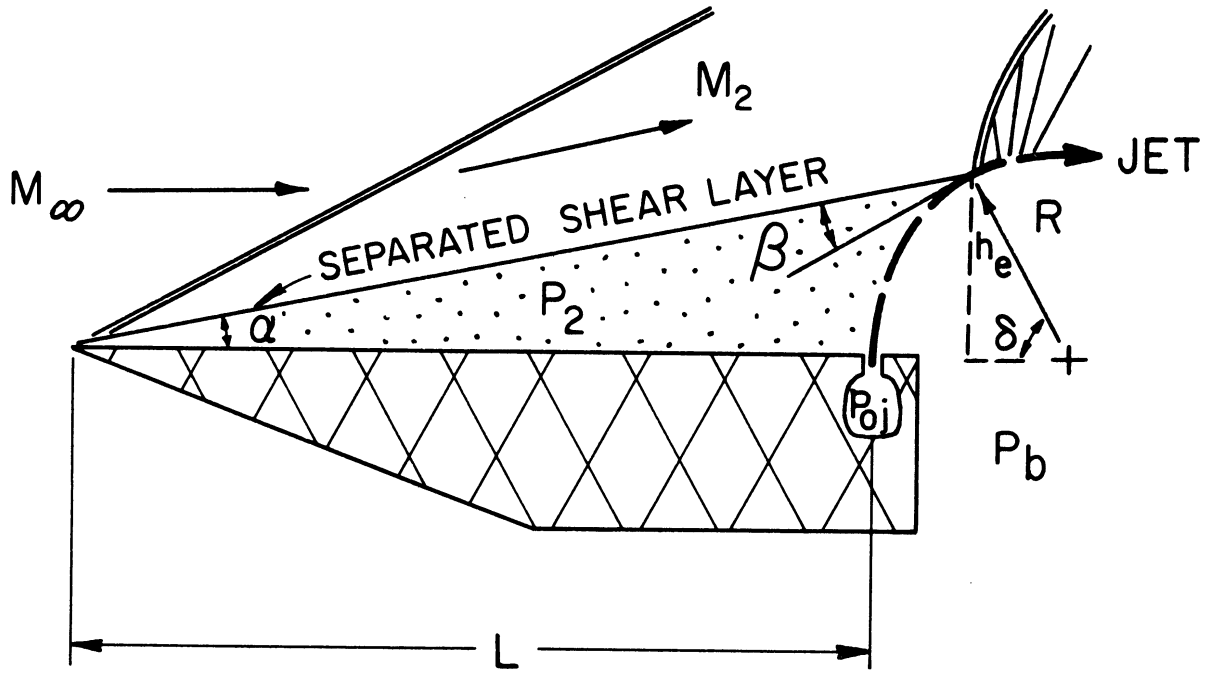

Fig. 12. Flow model.

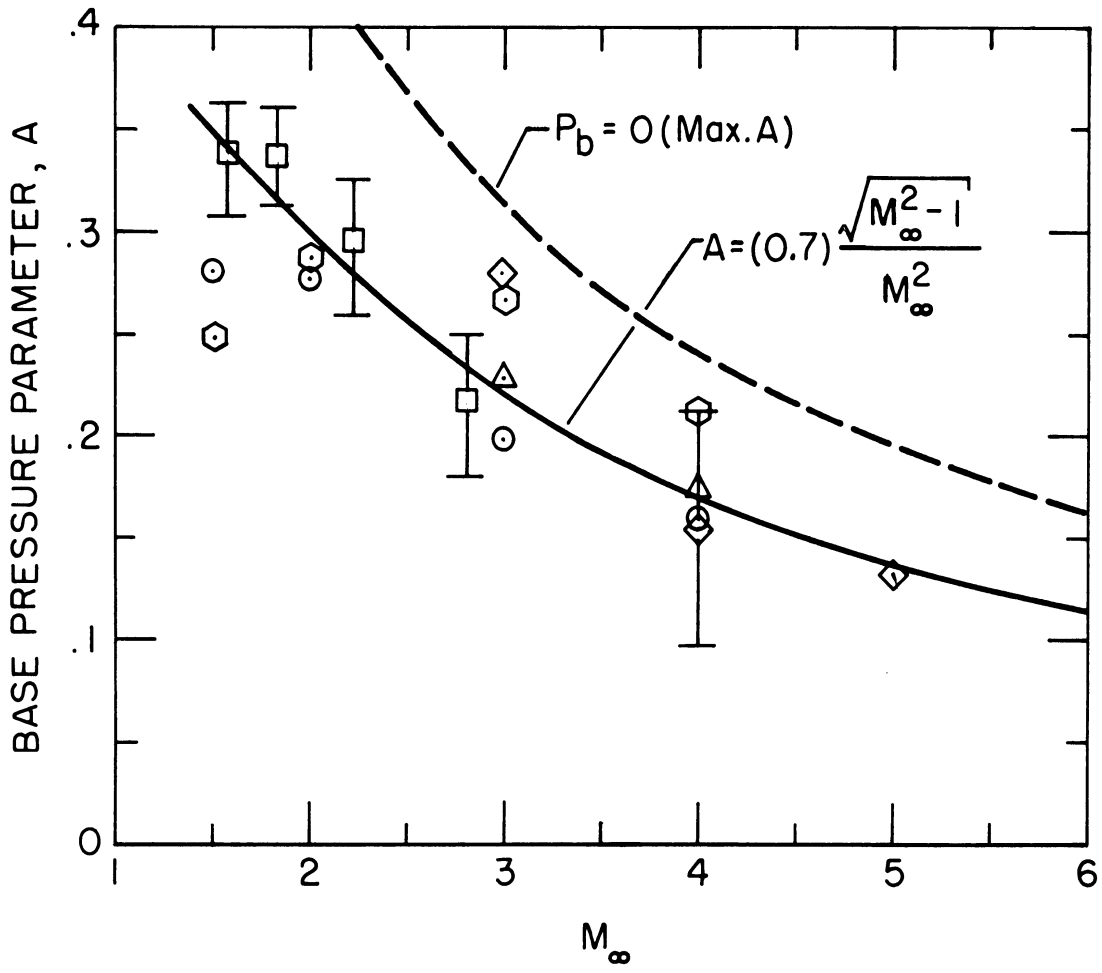

⊙ Wedge base, Ref. 8, $Re_L = .5 \times 10^6$, $t/L = .125$
△ " " Ref. 8, Re_L = " $t/L = .250$
⬡ " " Ref. 8, $Re_L \geq 3.0 \times 10^6$, Both thickness ratios.
⊡ Behind jet spoilers, Ref. 5
◇ " " " Ref. 3

Fig. 13. Base pressure parameter vs. Mach number.

UNIVERSITY OF MICHIGAN
3 9015 03026 8554